



Cite this: *New J. Chem.*, 2020, 44, 141

Catalytic formation of N3-substituted quinazoline-2,4(1*H*,3*H*)-diones by Pd(II)EN@GO composite and its mechanistic investigations through DFT calculations†

Surajit Biswas,^a Resmin Khatun,^{‡a} Malay Dolai,^{§a} Imdadul Haque Biswas,^a Najirul Haque,^a Manideepa Sengupta,^{ac} Md Sarikul Islam^a and Sk Manirul Islam^{id*}

In the current era, the scientific community is very much interested to utilize the greenhouse gas, carbon dioxide, through chemical fixation in order to produce value-based fine organic chemicals. The chemical combination of atmospheric carbon dioxide, isocyanides, and 2-iodoaniline in a one-pot reaction for the synthesis of quinazoline-2,4(1*H*,3*H*)-dione derivatives is a straight forward and attractive methodology to avoid multi-step and more toxic reagent containing routes. In this study, a heterogeneous catalyst was designed and synthesized from aminically modified graphene oxide by the incorporation of palladium metal. The catalyst was characterized by FT-IR, XRD, ICP-AES, Raman spectroscopy, XPS, TEM, SEM, EDX, and N₂ absorption desorption studies. In this report, the formation of N3-substituted 2,4(1*H*,3*H*)-quinazolinediones was performed under mild and heterogeneous reaction conditions under 1 bar CO₂ pressure. The catalyst is very efficient to produce the quinazoline derivatives. For the investigation of the mechanistic route of the catalytic reaction, density functional theory (DFT) calculations were also monitored. We have checked the recyclability of the catalyst, the results indicated that the catalyst maintained its catalytic efficacy even after six cycles of use.

Received 19th August 2019,
Accepted 15th November 2019

DOI: 10.1039/c9nj04288a

rsc.li/njc

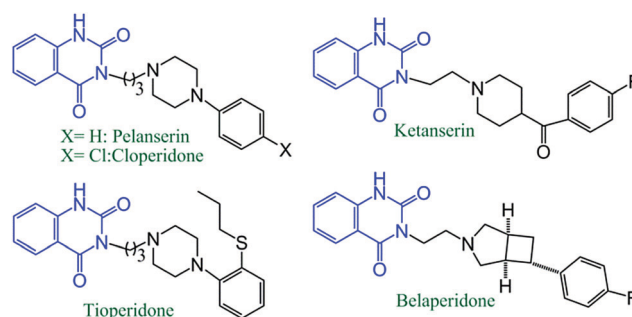
Introduction

In the last two decades, the scientific community has given increasing attention to the use of non-toxic, renewable, abundant, and inexpensive carbon dioxide for manufacturing value-based organic compounds.¹ Although a significant development has already been in progress in the related field, mainly by d-block metal-catalyzed reactions, the synthesis of heterocyclic compounds such as phenyl-annulated heteroarenes through carbon dioxide insertion has been less explored.²

Isocyanides have been largely used as important synthons in modern synthetic organic chemistry, particularly for N-containing heterocyclic compounds synthesis *via* chemical conversions, including multi-component reactions.^{3–7} Nowadays, various transition metal (such as Pd³, Cu⁴, Ag⁵, Co⁶ and Ni⁷) catalyzed reactions have been reported, where isocyanides are employed

for the production of N-containing heterocyclic molecules. Quinazoline-2,4(1*H*,3*H*)-diones are a very important structural sub-moiety of many commercially available drugs and biologically active molecules. Anti-hypertensive drugs such as cloperidone,⁸ pelanserine,⁹ ketanserine¹⁰ and anti-psychotic drugs including tioperidone¹¹ and belaperidone¹² all contain quinazoline-2,4(1*H*,3*H*)-diones as the prime framework (Scheme 1). Not only that these compounds are important intermediates for the production of bio-active N1,N3-disubstituted quinazoline-2,4(1*H*,3*H*)-diones and N3-substituted quinazoline-4(3*H*)-ones (Scheme 2).¹³

Traditionally, the synthesis of quinazoline-2,4(1*H*,3*H*)-diones involved more poisonous reagents [such as carbon monoxide,



Scheme 1 Quinazoline-2,4(1*H*,3*H*)-diones moiety in some drug molecules.

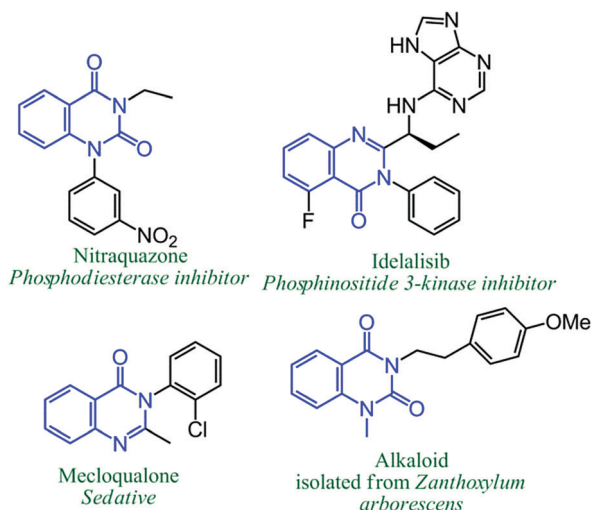
^a Department of Chemistry, University of Kalyani, Kalyani, Nadia 741235, West Bengal, India. E-mail: manir65@rediffmail.com; Fax: +91-33-2582-8282; Tel: +91-33-2582-8750

^b Department of Chemistry, Prabhat Kumar College, Purba Medinipur 721401, India

^c Refinery Technology Division, CSIR-Indian Institute of Petroleum, Dehradun, 248005, Uttarakhand, India

† Electronic supplementary information (ESI) available. See DOI: 10.1039/c9nj04288a

‡ These authors contributed equally.

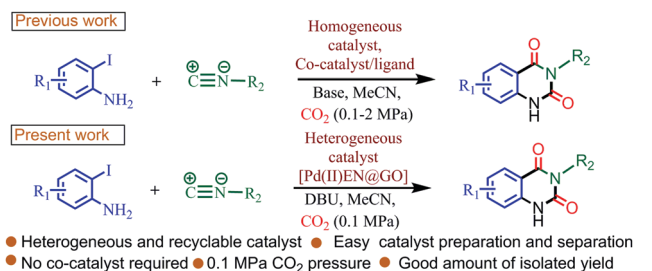


Scheme 2 Some examples of biologically active N1,N3-substituted quinazoline-2,4(1H,3H)-diones, and N3-substituted quinazoline-4(3H)-ones.

azides, phosgene/phosgene derivatives (di-*tert*-butyl dicarbonate, chloroformates, and isocyanates)]^{14–16} and multiple steps. Consequently, the low atom economy and the variation in the substituent in the arene ring were found to be very difficult. Thus, those synthetic procedures were not desirable from the point of both economical as well as environmental aspects, and hence an effective single-step low-cost route for the access of such an important skeleton molecule was highly demandable.

The combination of carbon dioxide and isocyanides *via* a multi-component reaction to manufacture N3-substituted 2,4(1H,3H)-quinazolin-2-one derivatives would be an attractive way, but in the participation of transition metal catalysts, this type of a multi-component reaction is still under development.¹⁷ This is because carbon dioxide is a gas and its solubility is very poor in organic solvents, and again with increasing temperature, the solubility decreases. Moreover, isocyanides are solids or liquids and completely soluble in organic solvents. As a result, the combination of both reactants (*i.e.* CO₂ and isocyanides) in the multi-component reaction becomes very challenging.

Herein, we reveal the design, synthesis, and characterizations of ethylenediamine-grafted GO-based palladium, Pd(II)EN@GO composite and its potential catalytic ability in a carboxylation–cyclization–insertion reaction to prepare N3-substituted 2,4(1H,3H)-quinazolin-2-one derivatives *via* a multi-component coupling of *o*-halo anilines, CO₂ and isocyanides. The catalytic reaction offers a methodology for the manufacture of N3-substituted 2,4(1H,3H)-quinazolin-2-one derivatives through the use of atmospheric CO₂ under mild reaction conditions (Scheme 3). Previously reported protocols regarding this synthesis involved homogeneous catalysts as well as the requirement of high pressure CO₂. Also, those protocols required the presence of some co-catalyst/ligand (Scheme 3). Again first-time density functional theory calculations were performed to investigate the mechanistic pathway of the catalytic reaction cycle. Moreover, the catalysis process occurred *via* a heterogeneous pathway and the catalyst was effective even after sixth consecutive cycles of utilization.



Scheme 3 Comparison between previous reports with the present study for the catalytic synthesis of N3-substituted quinazolin-2,4(1H,3H)-diones *via* carboxylation–cyclization–insertion reaction.

Experimental

Graphene oxide (GO) synthesis

Previously reported procedure¹⁸ was followed to synthesize graphene oxide. Concentrated H₃PO₄ (20 ml) and H₂SO₄ (180 ml) were taken in a 500 ml RB flask. 1.5 g of graphite flakes were added slowly to the solution. Then, potassium permanganate (9 g) was added pinch by pinch to the mixture. The resultant mixture was stirred at 50 °C for 16 hours. After completing the reaction, the mixture was cooled at RT. 30% H₂O₂ (3 ml) was added to the reaction solution and ice-cooled for a few hours until a brown coloration appeared. The obtained brown-colored solution was centrifuged and washed thoroughly by a 10% solution of hydrochloric acid, H₂O (de-ionized), and MeOH sequentially. Finally, the solid brown graphene oxide was desiccated in a vacuum.

Preparation of GO-EN

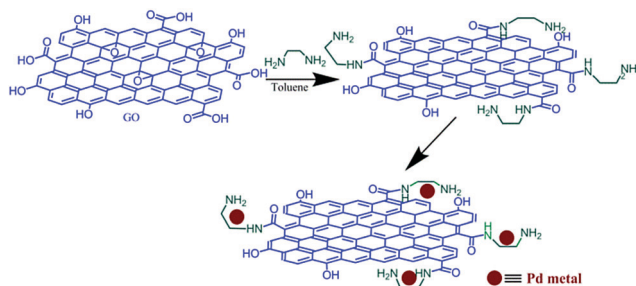
In toluene (80 ml), 1 g of GO powder was dispersed through sonication for 3 hours using an ultrasonic bath. Then, 25 ml of ethylenediamine and 4 ml of triethylamine were added, in sequence, to this solution. The resultant solution was heated to reflux under a N₂ atmosphere for 48 hours. Finally, the reaction mixture was cooled, filtered and washed successively using anhydrous toluene and MeOH to eliminate excess ethylenediamine and dried under vacuum.

Pd(II)EN@GO catalyst preparation

The obtained material (GO-EN) (1 g) was suspended in 60 ml of EtOH *via* sonication for 1 h. Then, 5 ml PdCl₂ solution (5% w/v) was added drop-wise to the solution and refluxed for 20 hours under stirring conditions. The final reaction mixture was centrifuged and washed using ethanol several times to eliminate the un-reacted PdCl₂, and finally Pd(II)EN@GO composite was dried under vacuum (Scheme 4).

General preparation of N3-substituted 2,4(1H,3H)-quinazolin-2-one derivatives

A mixture of 2-iodoaniline/derivatives (0.6 mmol, 1 equiv.), *tert*-butyl isocyanides/cyclohexyl isocyanides (0.72 mmol, 1.2 equiv.), 1,8-diazabicyclo[5.4.0]undec-7-ene (1.2 mmol, 2 equiv.) and 50 mg of Pd(II)EN@GO were taken in 4 ml of anhydrous MeCN in a 25 ml RB flask. The mixture was stirred under 1 atm of CO₂ using a balloon set up that was maintained at 80 °C temperature.



Scheme 4 Scheme for preparation of the Pd(II)EN@GO composite.

The progress of the reaction was monitored by thin-layer chromatography, and after completing the reaction, the solution was cooled and evaporated using a rotary evaporator. The separated pure product (*via* column chromatography) was identified by FT-IR and ^1H NMR spectroscopies.

Results and discussion

Ethylenediamine-modified graphene oxide-based palladium, Pd(II)EN@GO, composite was synthesized and characterized. In the first step, GO was produced by a previously reported method, and then it has been aminated by ethylenediamine molecules. Finally, the PdCl₂ solution (5% w/v) was used in order to get the Pd(II)EN@GO composite.

Characterization

FTIR spectra. A broadband is exhibited in the 2800–3750 cm⁻¹ range. The midpoint at 3400 cm⁻¹ in the FTIR spectra of graphene oxide was attributed to the –OH group stretching in the carboxylic acid functional groups, alcohol, and/or adsorbed water molecules (Fig. 1). Another four characteristics peaks of GO also appeared at 1740 cm⁻¹ (due to the stretching frequency of C=O present in the aldehyde, ketone, and carboxyl groups), 1626 cm⁻¹ (because of sp² C=C), 1058 and 1228 cm⁻¹ (for the stretching frequency of C–O associated with the epoxy and phenolic groups, respectively).¹⁹ In the GO-EN spectra, the band at 1740 cm⁻¹ of GO disappeared, and the intensity of the band in the 2800–3750 cm⁻¹ range decreased. Moreover three new peaks observed at 3080 cm⁻¹

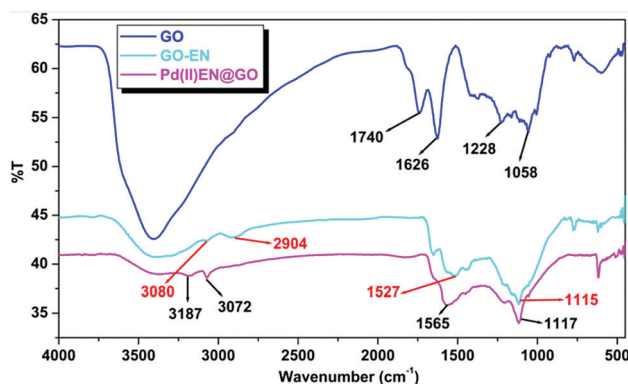


Fig. 1 Fourier-transform infrared spectra of graphene oxide, GO-EN, and Pd(II)EN@GO.

(–N–H stretching vibration of amine), 2904 cm⁻¹ (–CH stretching), and 1527 cm⁻¹ (–N–H bending vibration of amine)²⁰ clearly confirm the grafting of ethylenediamine onto the GO surface. In the case of the Pd(II)EN@GO composite, the position of all those peaks shifted to a higher wavenumber.

Powder X-ray diffraction studies. The PXRD studies of the graphene oxide and Pd(II)EN@GO composite is shown in Fig. 2. Two characteristics diffraction peaks at $2\theta = 10.001^\circ$ and 42.375° appeared in the PXRD spectra of graphene oxide. The peak at $2\theta = 10.001^\circ$ is because of the (002) plane of GO and the other peak at $2\theta = 42.375^\circ$ is due to the (100) plane of carbon hexagonal structure in GO.²¹ The (002) plane of graphene oxide shifted to a slightly higher angle of $2\theta = 11.348^\circ$ after the incorporation of both ethylenediamine and Pd metal on the GO surface. This plane shifting occurred due to the sonication and intercalation of molecules. There are also two new peaks that appeared in the spectra of Pd(II)EN@GO at $2\theta = 40.512^\circ$ and 46.327° , which correspond to the (111) and (200) planes of palladium.²² Therefore, it was confirmed that the Pd metal was incorporated on the surface of ethylenediamine modified graphene oxide sheets.

Raman spectra. In order to study the structural variation that arises during the course of a chemical reaction from graphene oxide to the Pd(II)EN@GO composite formation, Raman spectroscopy was performed. In the Raman spectrum of pure GO two characteristic peaks are observed, one is at 1598 cm⁻¹, which signifies the G band, and the other was at 1355 cm⁻¹, which implies the D band (Fig. 3). The D band is associated with structural deficiency and disorders, while the G band was connected to the E_{2g} phonon of sp²-C atoms stretching frequency in the graphene sheets.²³

The appearance of both D and G bands in the Pd(II)EN@GO composite's Raman spectrum confirmed the existence of the graphitic carbon in the composite. It was found from the previous reports that the intensity ratio of D and G bands (I_D/I_G) typically enhanced the interactions of electrons between metal nanoparticles or metal and graphene oxide when metal nanoparticles or metal are grafted on the graphene oxide surface.²⁴

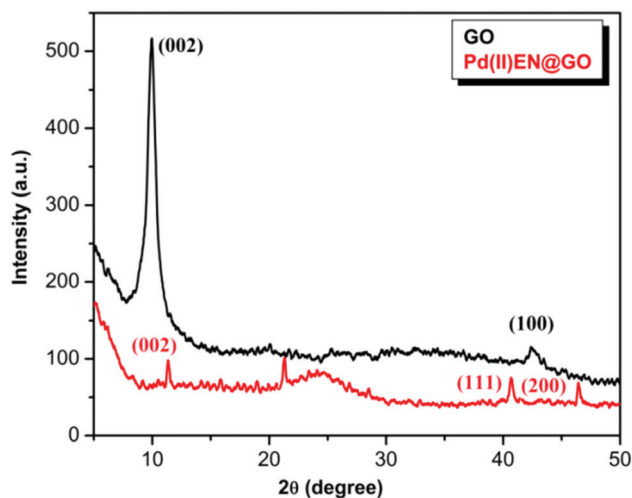


Fig. 2 X-ray powder diffraction spectra of graphene oxide and Pd(II)EN@GO.

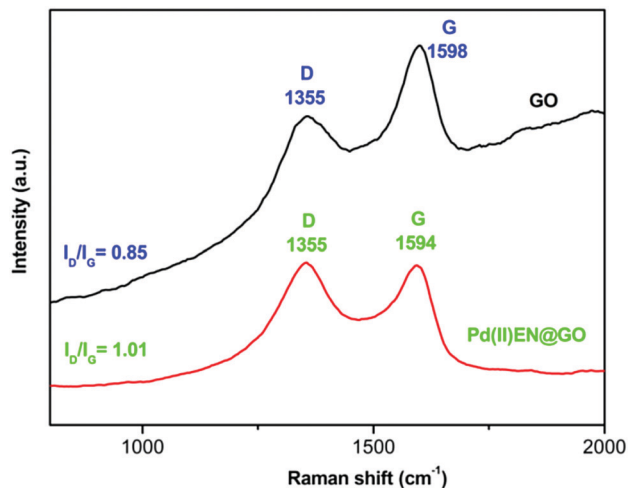


Fig. 3 Raman spectra of graphene oxide and Pd(II)EN@GO composite.

Here, the intensity ratio (I_D/I_G) of the composite increased to 1.01 from 0.85 (that of pure GO) and also shifting of the G band from 1598 cm^{-1} to 1594 cm^{-1} was observed. These results indicate the electronic interactions between Pd metal and aminically modified graphene oxide, thus confirming the successful attachment of the Pd metal on GO-EN.

FE SEM and HR TEM analysis. The FE SEM and HR TEM analyses were performed to predict the structure and morphology of the catalyst. The SEM images of the Pd(II)EN@GO composite (Fig. 4) disclosed a distinct 3D interconnected graphene sheet, having a sponge-like porous arrangement. The EDX spectrum coupled to the SEM established the presence of Pd in the catalyst texture (Fig. S1, ESI†).

The HR-TEM images with various higher magnification of the Pd(II)EN@GO composite are shown in Fig. 5. The images exposed transparent films of modified GO with net-like appearances.

Fig. 5(b) image illustrated the magnification part (red box part) of Fig. 5(a), whereas Fig. 5(c) pointed up that of Fig. 5(b) (white box part). The black spots in those images indicate the presence of the Pd metal particles, which are homogeneously distributed over the modified graphene oxide surface. The average particle size was around 3–4 nm.

Fig. 6 shows the elemental mapping of the composite. A consistent allocation of elements C, N, O, and Pd on the whole surface of GO indicates the steady attachments of the ethylenediamine on GO and desirable incorporation of the palladium

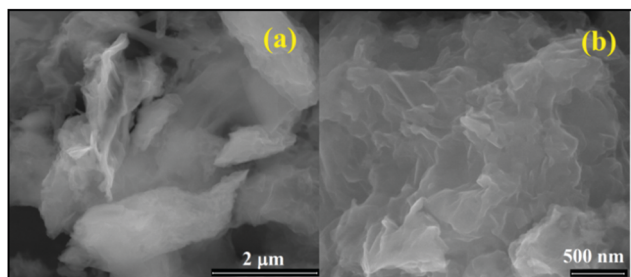


Fig. 4 FE-SEM images of the Pd(II)EN@GO composite.

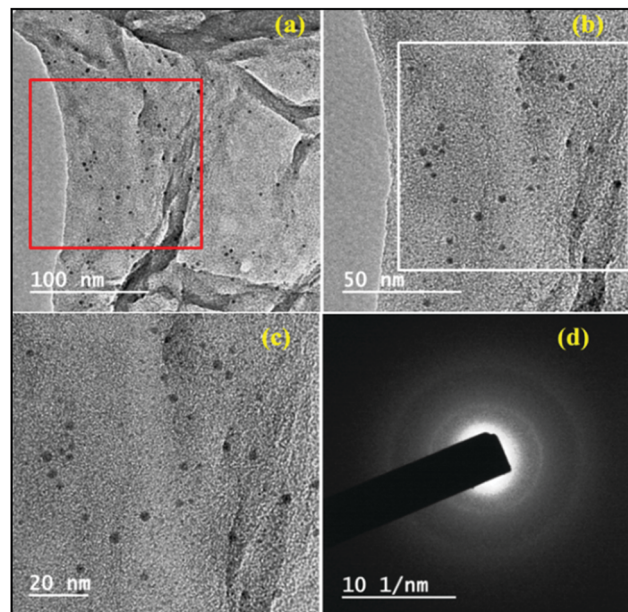


Fig. 5 HR-TEM images of the Pd(II)EN@GO composite.

metal. The EDX pattern obtained from HR TEM further confirmed the presence of carbon, nitrogen, oxygen, and palladium on the GO surface.

N₂ adsorption–desorption study. The N₂ adsorption–desorption study of the Pd(II)EN@GO catalyst was performed to investigate the pore size as well as the surface area of the catalyst. The catalyst isotherm depicts a typical type IV sorption isotherm, having a hysteresis loop nearly at a $0.8 < p/p_0 < 1.0$ pressure range (Fig. 7).²⁵ From the BJH method, the pore size distribution curve was plotted, and the plot clearly indicates that the catalyst contains typical pores with a size of 4.04 nm. Thus, the pore size of the material representing Pd(II)EN@GO was a class of mesoporous material. Again, from the BET analysis, we confirmed the catalyst surface area was $11.658\text{ m}^2\text{ g}^{-1}$.

X-ray photoelectron spectroscopy. To know the oxidation state of the palladium metal in the composite, X-ray photoelectron spectroscopy analysis was performed. The XPS spectrum of the 3d core-shell of palladium in the composite displays two

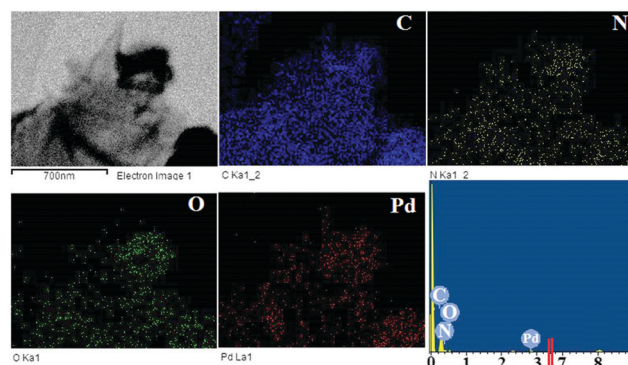


Fig. 6 Elemental mapping and EDX of the Pd(II)EN@GO composite from HR-TEM.

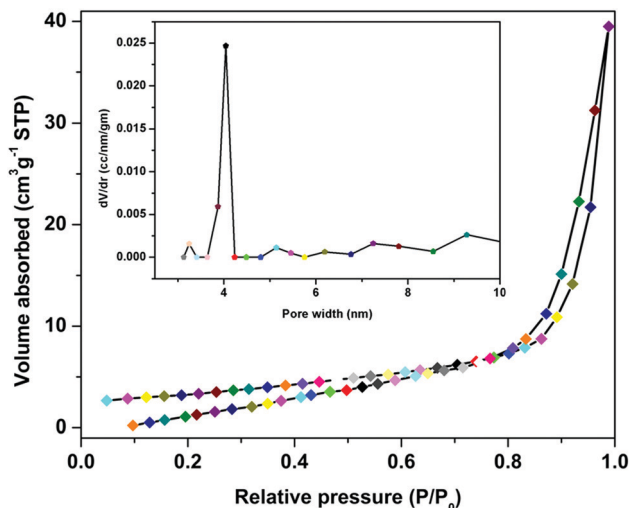


Fig. 7 N_2 adsorption-desorption isotherm of the Pd(II)EN@GO catalyst.

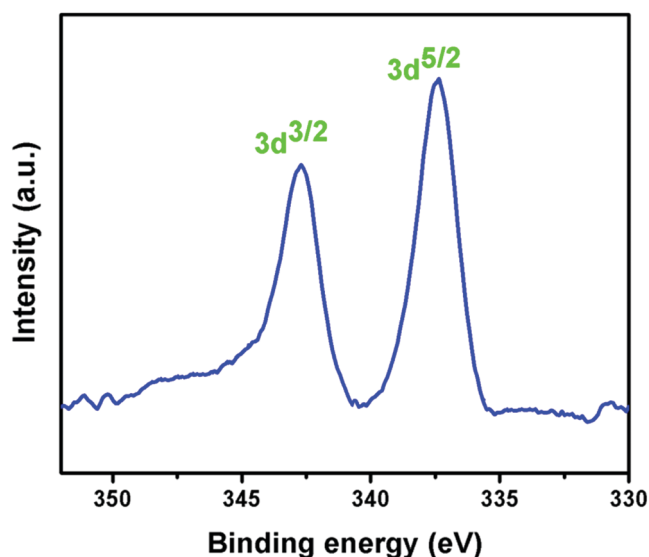


Fig. 8 X-ray photoelectron spectra of the Pd 3d level of the Pd(II)EN@GO catalyst.

peaks at 337.4 and 342.7 eV, which can be assigned to the binding energies of Pd 3d^{5/2} and Pd 3d^{3/2}, respectively (Fig. 8). These values imply that the presence of the Pd²⁺ species in the Pd(II)EN@GO composite.

The loading of the palladium(II) metal on the GO surface was also determined through the ICP-AES analysis, and the result suggested that about 7.13% of the palladium metal is present in the GO-EN surface.

Catalytic performance of the Pd(II)EN@GO catalyst

Formation of N3-substituted 2,4(1*H*,3*H*)-quinazolin-2(1*H*)-ones via three component coupling of *o*-halo anilines, CO₂ and isocyanides by the Pd(II)EN@GO catalyst. To determine the optimized reaction conditions, we varied various reaction factors such as solvent, base, temperature, catalyst amount, and time by performing the reaction of 2-iodoaniline (**R1**) with *tert*-butyl

isocyanide (**1a**) under atmospheric CO₂ pressure in the presence of the Pd(II)EN@GO catalyst as the model reaction. Initially, we performed the reaction using 2-iodoaniline (0.6 mmol), *tert*-butyl isocyanide (0.72 mmol, 1.2 equiv.), DBU (0.6 mmol, 1 equiv.) in 4 ml dry MeCN in the presence of a 40 mg catalyst at 80 °C under a 1 atm carbon dioxide pressure. To our delight, the reaction gave 64% isolated yield of the desired product (**P1**) (Table 1, entry 1). By changing the DBU amount from 1 equivalent to 2 or 3 equivalents with respect to the substrate under the same reaction conditions (Table 1, entries 2 and 3), we obtained a better yield (85%) of the product with the use of 2 equivalents of DBU. Then, we altered the base DBU with different organic bases, including 1,4-diazabicyclo[2.2.2]octane (DABCO), *N,N*-diisopropylethylamine (DIPEA), *t*-BuOK, NEt₃ or inorganic bases, including Cs₂CO₃, K₂CO₃, and K₃PO₄, (Table 1, entries 4–10) but did not get improve results compared with the use of the DBU base. Now the same reaction was monitored using 2 equiv. of DBU in various solvents (Table 1, entries 11–16), the collective data showed that MeCN was the most effective solvent for the catalytic reaction. Next, we varied the amount of catalyst (Table 1, entries 17–19), the highest yield of product (94%) was obtained after 10 h of reaction when 50 mg of Pd(II)EN@GO was used in the reaction (Table 1, entry 17).

Only 15% yield of the desired product was obtained in the absence of the catalyst, but in the presence of DBU (Table 1, entry 20) and without the base (DBU) in the presence of a

Table 1 Screening of reaction conditions^a

Entry	Solvent	Base (equiv.)	Amount of catalyst (mg)	Temp. (°C)	Time (h)	Yield ^b (%)
1	MeCN	DBU (1)	40	80	10	64
2	MeCN	DBU (2)	40	80	10	85
3	MeCN	DBU (3)	40	80	10	74
4	MeCN	DABCO (2)	40	80	5	42
5	MeCN	DIPEA (2)	40	80	5	38
6	MeCN	<i>t</i> -BuOK (2)	40	80	5	35
7	MeCN	NEt ₃	40	80	5	30
8	MeCN	Cs ₂ CO ₃ (2)	40	80	5	34
9	MeCN	K ₂ CO ₃	40	80	5	22
10	MeCN	K ₃ PO ₄	40	80	5	24
11	DMSO	DBU (2)	40	80	10	43
12	DMA	DBU (2)	40	80	10	38
13	DCE	DBU (2)	40	80	10	33
14	Toluene	DBU (2)	40	80	10	65
15	THF	DBU (2)	40	80	10	13
16	1,4-Dioxane	DBU (2)	40	80	10	52
17	MeCN	DBU (2)	50	80	10	94
18	MeCN	DBU (2)	30	80	10	60
19	MeCN	DBU (2)	60	80	10	87
20	MeCN	DBU (2)	—	80	5	15
21	MeCN	—	40	80	10	28
22	MeCN	—	—	80	10	00
23	MeCN	DBU (2)	50	90	10	76
24	MeCN	DBU (2)	50	70	10	48

^a Reaction conditions: 2-iodoaniline, **R1** (0.6 mmol), *t*-BuNC, **1a** (0.72 mmol), solvent (4 ml), base, catalyst, CO₂ balloon. ^b Isolated yields.

Table 2 Substrate scope^a

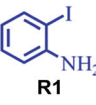
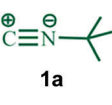
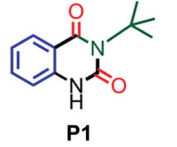
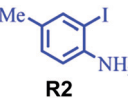
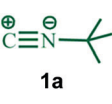
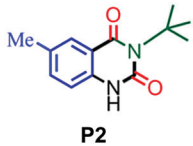
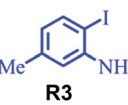
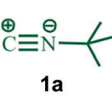
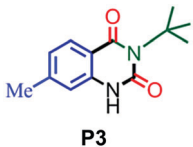
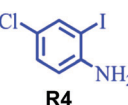
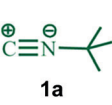
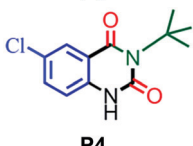
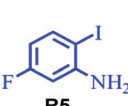
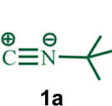
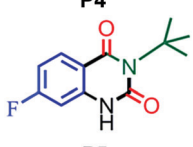
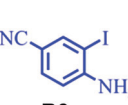
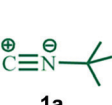
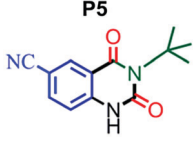
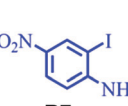
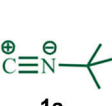
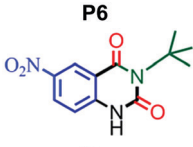
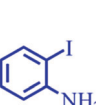

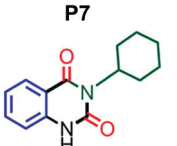
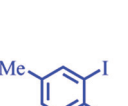

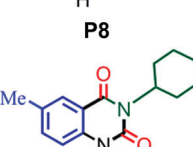
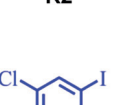

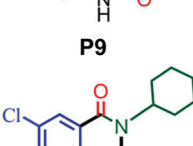
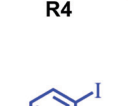

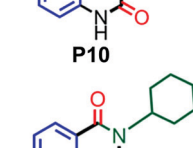
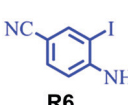

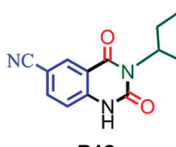
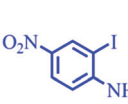

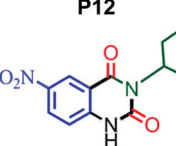
Entry	Substrate	Isocyanides	Product	Yield ^b (%)
1				94
2				95
3				93
4				88
5				85
6				65
7				55
8				92
9				94
10				83
11				80

Table 2 (continued)

Entry	Substrate	Isocyanides	Product	Yield ^b (%)
12				64
13				58

^a Reaction conditions: substrate (0.6 mmol), isocyanide (0.72 mmol), Pd(II)EN@GO (50 mg, 0.033 mmol based on the Pd metal), DBU (1.2 mmol), MeCN (4 ml), 80 °C, carbon dioxide balloon, 10 hours.
^b Isolated yields.

catalyst (40 mg) only ~28% of the desired product was formed (Table 1, entry 21). Again in the absence of both catalysts and base, no conversion of the substrate was observed (Table 1, entry 22). Lastly, the temperature effect on the reaction was checked (Table 1, entries 23 and 24), the results demonstrated that 80 °C is the optimum temperature for the reaction. Therefore, the optimized reaction condition for the reaction was: substrate (0.6 mmol), *t*-BuNC (0.72 mmol), Pd(II)EN@GO (50 mg, 0.033 mmol based on the Pd metal), DBU (1.2 mmol, 2 equiv.), MeCN (4 ml), 80 °C, carbon dioxide (1 atm).

Under the optimized reaction conditions, we investigated the substrate scope of various derivatives of *o*-iodoanilines (Table 2). An electron-donating group (such as methyl group) containing 2-iodoanilines afforded >90% isolated yield of the corresponding desired product through this reaction. When mild electron-withdrawing groups such as cyano, chloro, or fluoro-substituted *o*-iodoanilines were subjected to the reaction, we got moderate to very good isolated yield (65–88%) of the respective product. Moreover, strong electron-withdrawing –NO₂ substituted 2-iodoaniline derivative also produced a 55% yield of the corresponding quinazolin-5(1H)-one product.

Under the same optimized reaction conditions, all derivatives of 2-iodoaniline furnished a mild to excellent isolated yield (58–94%) when cyclohexyl isocyanide was used instead of *tert*-butyl isocyanide (Table 2).

So far, only three protocols were developed for the catalytic production of N3-substituted 2,4(1*H*,3*H*)-quinazolin-5(1*H*)-ones via a three-component coupling reaction of isocyanide, 2-haloaniline, and carbon dioxide in the presence of a palladium metal catalyst.¹⁷ All three protocols produced the desired products with high yield under mild reaction conditions but in a homogeneous catalytic environment and in the presence of a co-catalyst/ligand (Table 3). Therefore, the recyclability and reusability of the catalyst remain problematic in those catalytic systems. In our developed protocol, the catalytic reactions occurred in a heterogeneous condition under mild reaction conditions and 1 atm CO₂ pressure. Again no co-catalyst/ligand was required in this method. Moreover, the catalyst was easily recyclable and reusable.

Table 3 Comparison table of the catalytic synthesis of 3-(*tert*-butyl)quinazoline-2,4(1*H*,3*H*)-dione (**P1**) via the coupling reaction of 2-iodoaniline, carbon dioxide and *tert*-butyl isocyanide with other reported methods

Serial no.	Catalyst	Reaction conditions	Catalytic nature	T (h)	Yield (%)	Ref.
1	Pd(CH ₃ CN) ₂ Cl ₂	2-Iodoaniline (0.20 mmol), <i>tert</i> -butyl isocyanide (0.24 mmol), catalyst (10 mol%), SPhos (20 mol%), Cs ₂ CO ₃ (0.40 mmol), CO ₂ (2 MPa), DMSO (4 ml), 90 °C	Homogeneous	12	90	17a
2	Pd(OAc) ₂	2-Iodoaniline (0.50 mmol), <i>t</i> -BuNC (0.60 mmol), catalyst (3 mol%), diadamantylbutylphosphine (6 mol%), Cs ₂ CO ₃ (1.0 mmol), 1,4-dioxane (1.0 ml), carbon dioxide (10 atm), 80 °C.	Homogeneous	7	94	17b
3	PdCl ₂	2-Iodoaniline (0.30 mmol), <i>tert</i> -butyl isocyanide (0.45 mmol), catalyst (0.03 mmol), DBU (0.6 mmol), triphenylphosphine (0.06 mmol), dry acetonitrile (2 ml), carbon dioxide balloon, 80 °C	Homogeneous	12	92	17c
4	Pd(II)EN@GO	2-Iodoaniline (0.6 mmol), <i>tert</i> -butyl isocyanide, (0.72 mmol), Pd(II)EN@GO (50 mg, 0.033 mmol based on Pd metal), DBU (1.2 mmol), MeCN (4 ml), CO ₂ balloon, 80 °C	Heterogeneous	10	94	This work

DFT calculation

To study and understand the mechanistic pathway of the current catalytic study from the molecular level, the density functional theory (DFT) computations were performed through GAUSSIAN 09.²⁶ First, the stabilization energies of the Pd(II)EN@GO composite (considering the GO composite as the methyl group) were computed, since the XRD and XPS results confirmed the presence of Pd(II) in the EN@GO composite, hence the DFT calculations were performed with Pd(II)EN@CH₃ as the active centre. The individual roles of the catalyst and support have been studied. All the ground state geometries were optimized without any symmetry constraints. All calculations were performed using the B3LYP function^{27,28} and LanL2DZ basis because it was confirmed²⁹ that for the transition metal this combination yields proper geometries and electronic properties. The stabilization of Pd(II)EN@GO {–CH₃≡GO} from the Pd(II)EN@GO composite was studied. For this study, only a portion of the Pd(II)EN@CH₃ was chosen for the simplicity of computation.

The absorption energy of Pd(II)EN@CH₃ was –237.765 kcal mol^{–1} and it was observed that Pd(II) was stabilized by the ethylene diamine (EN group) of the EN@GO composite, and two chlorine (Cl[–]) atoms attained a square planar geometry (Fig. 9). To understand the mechanistic pathway of the reaction along with the role of catalyst, reagent and base, a plausible mechanism for *o*-iodoaniline and *t*-BuNC cycloaddition with CO₂ in presence of the catalyst Pd(II)EN@CH₃, and a base DBU has been represented in Fig. 10, which was further confirmed from the DFT calculations. From the systematic study, it was clear that *o*-iodoaniline and *tert*-butyl isocyanide were not reactive to CO₂. However, the addition of the catalyst with *o*-iodoaniline and then *tert*-butyl isocyanide accelerated the catalysis of cycloaddition with CO₂; however, the lone pair of the coordinated aniline-catalyst moved towards the terminal carbon of CO₂, and ultimately provided the catalytic product (*Z*)-4-(*tert*-butylimino)-1*H*-benzo[d][1,3]oxazin-2(4*H*)-one. Simultaneously, this catalytic product undergoes a specific rearrangement in the presence of 1,8-diazabicyclo[5.4.0]undec-7-ene as a base to give the desired product 3-(*tert*-butyl)quinazoline-2,4(1*H*,3*H*)-dione.

At the beginning of the catalysis, catalyst Pd(II)EN@CH₃ becomes Pd(0)EN@CH₃ after the removal of two chlorine atoms as a Cl₂ molecule. Then, *o*-iodoaniline coordinates with this

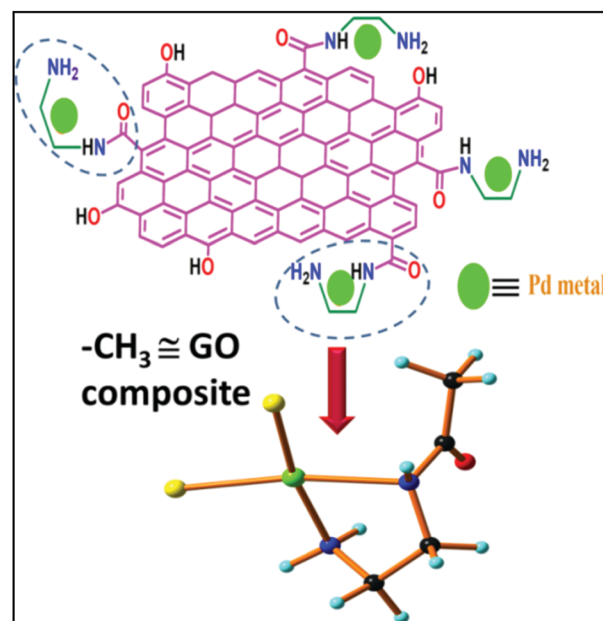


Fig. 9 Stabilization of Pd(II) metal coordination with EN@GO finally resulted in the Pd(II)EN@GO{–CH₃≡GO} composite.

Pd(0)EN@CH₃ through iodine and forms the transition state-1 (Fig. 11b), which is very reactive and enforces to create intermediate-1 (Fig. 11c). The intermediate-1 is then attacked by *tert*-butyl isocyanide to form the transition state-2 (Fig. 11d). Due to the strong repulsion of the ring electron, such transition states would not exist and the energy is very high so it is reactive.

Thus, the coordination of the lone pair of nitrogen of the amine group to CO₂ was activated on the opposite side. The formation of the transition state-2 was very reactive to CO₂. CO₂ first acted as a ligand and coordinated to Pd(II) via the O-atom, which enhanced the π -accepting capacity of the carbon dioxide's carbon and formed the intermediate-2 (Fig. 11e). The coordination of CO₂ to Pd(II) helps to push back the Pd–C(isocyanide) bond pair towards oxygen, which assists the formation of the C–CO₂ bond to form the intermediate of this reaction. Finally, the intermediate cyclizes to give the product (Fig. 11f) after the completion of catalysis. After that, this product was rearranged by the use of DBU as the base to give intermediate-3 (Fig. 12b) and finally gives

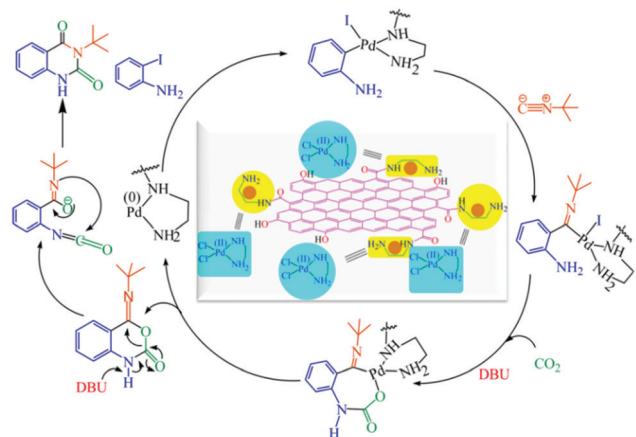


Fig. 10 Plausible mechanistic route for the preparation of 3-(*tert*-butyl)-quinazoline-2,4(1*H*,3*H*)-dione from *o*-iodoaniline, *tert*-butyl isocyanide, and atmospheric CO₂, via cycloaddition using the Pd(II)EN@GO composite as catalyst and DBU as a base.

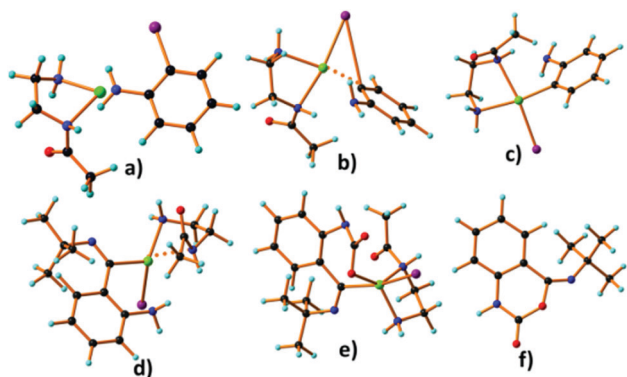


Fig. 11 (a) Reactant, (b) transition state-1, (c) intermediate-1, (d) transition state-2, (e) intermediate-2 and (f) catalytic product (Z)-4-(*tert*-butylimino)-1*H*-benzo[d][1,3]oxazin-2(4*H*)-one.

the desired product (Fig. 12c). To compare the effect of the Pd(II) ion, the reaction in the presence and absence of a catalyst was studied. It was observed that without a catalyst no reaction occurred.

The energy profile diagram for this reaction is shown in Fig. 13. The activation energy for the activation of *o*-iodoaniline to form TS-1 was 1.95 eV (45.40 kcal mol⁻¹). The free energy of the formation of the intermediate-1 was -8.07 eV (-187.90 kcal mol⁻¹). The activation energy for the attack of *tert*-butyl isocyanide to intermediate-1 to form TS-2 was 2.90 eV (67.52 kcal mol⁻¹). The free energy for the formation of the intermediate-2 from the reaction of TS-2 and CO₂ was -6.89 eV (-160.43 kcal mol⁻¹). The activation energy of cyclization was -9.17 eV (-213.52 kcal mol⁻¹). The catalytic product was rearranged to give (Z)-*N'*-*tert*-butyl-2-isocyanato-benzoxylimide (intermediate-3). The activation energy for the intermediate-3 was -9.29 eV (-216.54 kcal mol⁻¹) and finally, the free energy for the formation of the desired product was -9.10 eV (-211.99 kcal mol⁻¹). From the energy profile diagram, it was obvious that the first step was the rate-determining step of this reaction.

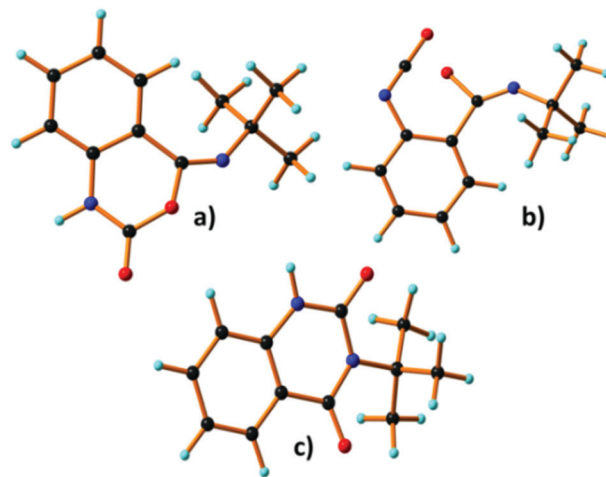


Fig. 12 The catalytic effect of the Pd(II)EN@GO composite in CO₂ cycloadditions with *o*-iodoaniline and *tert*-butyl isocyanide: yield as intermediates (a) (Z)-4-(*tert*-butylimino)-1*H*-benzo[d][1,3]oxazin-2(4*H*)-one, (b) formed (Z)-*N'*-*tert*-butyl-2-isocyanato-benzoxylimide after treatment of (a) with base DBU, (c) desired product 3-(*tert*-butyl)quinazoline-2,4(1*H*,3*H*)-dione.

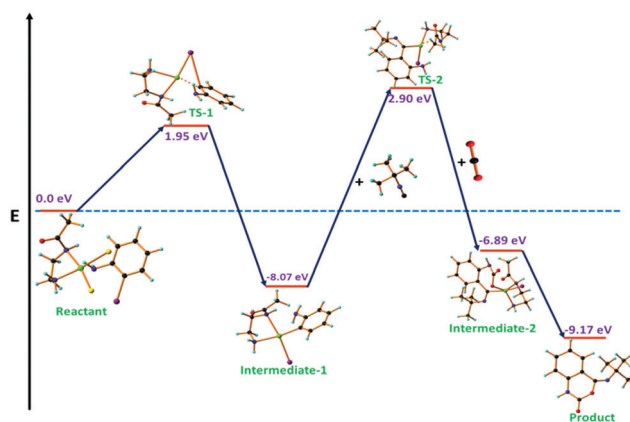


Fig. 13 Energy profile diagram for different transition states and intermediates for the generation of (Z)-4-(*tert*-butylimino)-1*H*-benzo[d][1,3]oxazin-2(4*H*)-one from *o*-iodoaniline, *tert*-butyl isocyanide and CO₂ in the presence of catalyst Pd(II)EN@GO composite.

From the DFT optimization, we found that the size of the substrate (*i.e.* 2-iodoaniline) was 2.79 nm, which was smaller than the pore size (4.04 nm) of the as-synthesized Pd(II)EN@GO catalyst. Therefore, it is clear from the DFT analysis that the substrate was completely incorporated into the pores of the catalyst material and got efficiently activated. In addition, we found that the size of the product (*i.e.* 3-*tert*-butylquinazoline-2,4(1*H*,3*H*)-dione) was 4.67 nm, which is larger than the catalyst pore size. This observation suggests that the product material does not block the pores of the catalyst material, which is in line with the efficient recyclability of the Pd(II)EN@GO catalyst.

Heterogeneity of catalyst

The life span in the industrial applications of a heterogeneous catalyst is its most essential features. So, to check the

heterogeneity of our synthesized catalyst, we performed a hot filtration test *via* the synthesis of 3-*tert*-butylquinazoline-2,4(1*H*,3*H*)-dione from *o*-iodoaniline, *tert*-butyl isocyanide and CO₂ in the presence of the Pd(II)EN@GO composite catalyst. Initially, the reaction was continued for 5 h under optimized reaction conditions; 64% yield of the desired product was obtained. Then, the catalyst was separated by filtration, and the reaction mixture without catalyst was further put into the same reaction environment for another 5 h. No significant change in the product yield was observed. After performing the filtration test, the filtrate was analyzed by ICP-AES but there was no trace of the palladium metal found in the filtrate. Moreover, FE SEM, IR, and XPS analyses of the recycled catalyst were performed for additional clarification. The FE SEM images of the reused catalyst showed almost the same morphology as that found in the fresh catalyst (Fig. S14, ESI†). No major change was detected in the peak position of the palladium metal in the XPS analysis of the recovered Pd(II)EN@GO catalyst (Fig. S15, ESI†). Two distinct peaks at 337.8 and 343.1 eV, which were due to the binding energies of Pd 3d^{5/2} and Pd 3d^{3/2} clearly indicate that the oxidation state of palladium *i.e.* +2 remains unchanged after finishing the catalysis³⁰ process. The inferred spectrum pattern of both the reused and fresh catalyst showed almost the same nature (Fig. S16, ESI†). This result signifies that after the catalytic reaction the nature of the catalyst remains unaltered. Again the ICP-AES analysis results of the used catalyst after the first cycle of the catalytic reaction gave the same result as the synthesized catalyst. Furthermore, the same analysis of the reused catalyst after the sixth cycle (Pd loading is 7.10%) did not show a considerable loss of the palladium metal amount from the GO-EN surface. The ICP analysis was also performed for the product mixtures of catalysis reaction, and the result confirmed the absent of palladium metal in the mixture. All these data confirm that the Pd metal was not leached from the catalyst during the course of the catalytic cycle, and hence the catalyst was conveyed in its heterogeneous nature throughout the reaction.

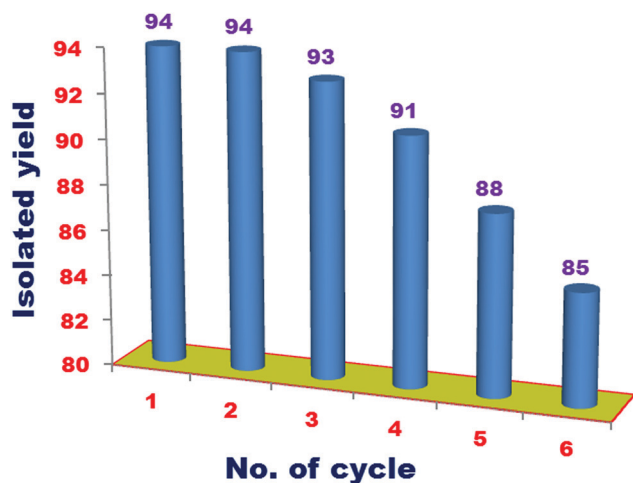


Fig. 14 Recyclability of catalyst for the synthesis of 3-(*tert*-butyl)-quinazoline-2,4(1*H*,3*H*)-dione (**P1**) *via* a three-component coupling of 2-iodoaniline, CO₂ and *tert*-butyl isocyanide.

Recycling of catalyst

Recyclability, recoverability and easy separation are the prime features of a heterogeneous catalyst. The catalyst recyclability was tested in a three-component coupling reaction of 2-iodoaniline, carbon dioxide, and *tert*-butyl isocyanide. From the reaction mixture, the catalyst was separated *via* a simple filtration after every catalytic cycle. Then, the separated catalyst was washed properly using distilled H₂O, hot MeOH, and acetone, and dried using a vacuum desiccator. Fig. 14 shows that after the use of six successive cycles, the catalyst maintains its efficiency.

Conclusion

Ethelenediamine-modified graphene oxide-based palladium metal-containing catalyst was designed and synthesized. The characterization of the catalyst was done *via* ICP-AES, PXRD, SEM, TEM, EDX, XPS, N₂ adsorption desorption, Raman and IR studies. The catalyst was very much efficient for the synthesis of N3-substituted quinazoline-2,4(1*H*,3*H*)-diones through a three-component coupling reaction of *o*-halo anilines, CO₂ and isocyanides. The catalytic reaction occurred in 1 bar CO₂ pressure under heterogeneous and mild reaction conditions. All previously reported methods regarding N3-substituted quinazoline-2,4(1*H*,3*H*)-diones synthesis, was proceeded under homogeneous catalytic conditions. Again, the high pressure of CO₂ was used. A mechanistic route for the catalytic cycles was reported here the first time *via* the DFT calculations. Besides, our catalyst is very stable, easily separable and preserved its catalytic efficiency after the use of six successive catalytic cycles.

Conflicts of interest

There are no conflicts to declare.

Acknowledgements

Prof. S. M. Islam acknowledges the Department of Science and Technology (DST-SERB) (Project sanction No. EMR/2016/004956), New Delhi, India, Board of Nuclear Science, (BRNS, project sanction number; 37(2)/14/03/2018-BRNS/37003), Govt of India and Council of Scientific and Industrial Research (CSIR, Project sanction No. 02(0284)/16/EMR-II, Dated 06-12-2016), and New Delhi, India for financial support. Dr S. Biswas acknowledges University Grants Commission (UGC) for financial support through D. S. Kothari Post-Doctoral Fellowship (Award letter no. F.4-2/2006(BSR)/CH/16-17/0026). R. Khatun also acknowledges UGC for providing the financial support through the Maulana Azad National Fellowship and the Department of Science and Technology (DST-INSPIRE) for financial support (INSPIRE fellow Registration No. IF170931) gratefully acknowledged by Md S. Islam. We acknowledge UGC and DST New Delhi, India for financial and instrumental support to the Department of Chemistry, the University of Kalyani under PURSE, FIST and SAP program. For providing Powder X-ray Diffraction instrument facility, we are very grateful to Dr Arup Gayen, Department of Chemistry, Jadavpur University, 188, Raja S. C. Mallick Rd, Kolkata 700032, West Bengal, India.

Notes and references

- 1 (a) Y.-G. Chen, X.-T. Xu, K. Zhang, Y.-Q. Li, L.-P. Zhang, P. Fang and T.-S. Mei, *Synthesis*, 2018, 35–48; (b) B. Yu, B. Zou and C.-W. Hu, *J. CO₂ Util.*, 2018, **26**, 314–322; (c) Z. Zhang, T. Ju, J.-H. Ye and D.-G. Yu, *Synlett*, 2017, 741–750; (d) M. Börjesson, T. Moragas, D. Gallego and R. Martin, *ACS Catal.*, 2016, **6**, 6739–6749; (e) B. Yu and L.-N. He, *ChemSusChem*, 2015, **8**, 52–62; (f) Q. Liu, L. Wu, R. Jackstell and M. Beller, *Nat. Commun.*, 2015, **6**, 5933–5948; (g) M. He, Y. Sun and B. Han, *Angew. Chem., Int. Ed.*, 2013, **52**, 9620–9633; (h) M. Cokoja, C. Bruckmeier, B. Rieger, W. A. Herrmann and F. E. Kühn, *Angew. Chem., Int. Ed.*, 2011, **50**, 8510–8537; (i) J.-L. Wang, C.-X. Miao, X.-Y. Dou, J. Gao and L.-N. He, *Curr. Org. Chem.*, 2011, **15**, 621–646.
- 2 (a) T. Niemi, I. Fernandez, B. Steadman, J. K. Mannisto and T. Repo, *Chem. Commun.*, 2018, **54**, 3166–3169; (b) V. B. Saptal and B. M. Bhanage, *ChemSusChem*, 2017, **10**, 1145–1151; (c) U. R. Seo and Y. K. Chung, *Green Chem.*, 2017, **19**, 803–808; (d) T. Niemi, J. E. Perea-Buceta, I. Fernández, O.-M. Hiltunen, V. Salo, S. Rautiainen, M. T. Räisänen and T. Repo, *Chem. – Eur. J.*, 2016, **22**, 10355–10359; (e) S. Sun, W.-M. Hu, N. Gu and J. Cheng, *Chem. – Eur. J.*, 2016, **22**, 18729–18732; (f) S. Wang, P. Shao, G. Du and C. Xi, *J. Org. Chem.*, 2016, **81**, 6672–6676; (g) K. B. Rasal and G. D. Yadav, *RSC Adv.*, 2016, **6**, 111079; (h) Z. Xin, C. Lescot, S. D. Friis, K. Daasbjerg and T. Skrydstrup, *Angew. Chem., Int. Ed.*, 2015, **54**, 6862–6866; (i) Y. Zhao, B. Yu, Z. Yang, H. Zhang, L. Hao, X. Gao and Z. Liu, *Angew. Chem., Int. Ed.*, 2014, **53**, 5922–5925; (j) C.-X. Guo, W.-Z. Zhang, S. Liu and X.-B. Lu, *Catal. Sci. Technol.*, 2014, **4**, 1570–1577; (k) K. Sasano, J. Takaya and N. Iwasawa, *J. Am. Chem. Soc.*, 2013, **135**, 10954–10957; (l) T. Ishida, S. Kikuchi and T. Yamada, *Org. Lett.*, 2013, **15**, 3710–3713; (m) T. Mizuno, M. Mihara, T. Nakai, T. Iwai and T. Ito, *Synthesis*, 2007, 2524–2528.
- 3 (a) W. Hu, J. Li, Y. Xu, J. Li, W. Wu, H. Liu and H. Jiang, *Org. Lett.*, 2017, **19**, 678–681; (b) G. C. Senadi, T.-Y. Lu, G. K. Dhandabani and J.-J. Wang, *Org. Lett.*, 2017, **19**, 1172–1175; (c) G. Qiu, Q. Wang and J. Zhu, *Org. Lett.*, 2017, **19**, 270–273; (d) Q. Yang, C. Li, M. X. Cheng and S.-D. Yang, *ACS Catal.*, 2016, **6**, 4715–4719; (e) Z. B. Chen, Y. Zhang, Q. Yuan, F. L. Zhang, Y. M. Zhu and J. K. Shen, *J. Org. Chem.*, 2016, **81**, 1610–1616; (f) G. Qiu, M. Mamboury, Q. Wang and J. Zhu, *Angew. Chem., Int. Ed.*, 2016, **55**, 15377–15381; (g) W. Kong, Q. Wang and J. Zhu, *Angew. Chem., Int. Ed.*, 2016, **55**, 9714–9718; (h) J. Peng, Y. Gao, W. Hu, Y. Gao, M. Hu, W. Wu, Y. Ren and H. Jiang, *Org. Lett.*, 2016, **18**, 5924–5927; (i) J. Li, Y. He, S. Luo, J. Lei, J. Wang, Z. Xie and Q. Zhu, *J. Org. Chem.*, 2015, **80**, 2223–2230; (j) Y.-Y. Pan, Y.-N. Wu, Z.-Z. Chen, W.-J. Hao, G. Li, S.-J. Tu and B. Jiang, *J. Org. Chem.*, 2015, **80**, 5764–5770; (k) G. C. Senadi, W.-P. Hu, S. S. K. Boominathan and J.-J. Wang, *Chem. – Eur. J.*, 2015, **21**, 998–1003; (l) Z.-Y. Gu, X. Wang, J.-J. Cao, S.-Y. Wang and S.-J. Ji, *Eur. J. Org. Chem.*, 2015, 4699–4709.
- 4 (a) D. Li, T. Mao, J. Huang and Q. Zhu, *Chem. Commun.*, 2017, **53**, 1305–1308; (b) K. Takamatsu, K. Hirano and M. Miura, *Org. Lett.*, 2015, **17**, 4066–4069; (c) J. Lei, X. Wu and Q. Zhu, *Org. Lett.*, 2015, **17**, 2322–2325; (d) S. Kim and S. H. Hong, *Adv. Synth. Catal.*, 2015, **357**, 1004–1012; (e) X. Huang, S. Xu, Q. Tan, M. Gao, M. Li and B. Xu, *Chem. Commun.*, 2014, **50**, 1465–1468; (f) P. Mampuy, Y. Zhu, T. Vlaar, E. Ruijter, R. V. A. Orru and R. B. U. W. Maes, *Angew. Chem., Int. Ed.*, 2014, **53**, 12849–12854; (g) B. Pooi, J. Lee, K. Choi, H. Hirao and S. H. J. Hong, *Org. Chem.*, 2014, **79**, 9231–9245; (h) C. Kanazawa, S. Kamijo and Y. Yamamoto, *J. Am. Chem. Soc.*, 2006, **128**, 10662.
- 5 (a) Y. Liu, X.-L. Chen, F.-L. Zeng, K. Sun, C. Qu, L.-L. Fan, Z.-L. An, R. Li, C.-F. Jing, S.-K. Wei, L.-B. Qu, B. Yu, Y.-Q. Sun and Y.-F. Zhao, *J. Org. Chem.*, 2018, **83**, 11727–11735; (b) Z. Hu, J. Dong, Y. Men, Z. Lin, J. Cai and X. Xu, *Angew. Chem., Int. Ed.*, 2017, **56**, 1805–1809; (c) X. Zhang, X. Wang, Y. Gao and X. Xu, *Chem. Commun.*, 2017, **53**, 2427–2430; (d) H. Wang, R. K. Kumar, Y. Yu, L. Zhang, Z. Liu, P. Liao and X. Bi, *Chem. – Asian J.*, 2016, **11**, 2841–2845; (e) J. Liu, Z. Liu, P. Liao, L. Zhang, T. Tu and X. Bi, *Angew. Chem., Int. Ed.*, 2015, **54**, 10618–10622; (f) J. Liu, Z. Liu, N. Wu, P. Liao and X. Bi, *Chem. – Eur. J.*, 2014, **20**, 2154–2158.
- 6 (a) Z.-Y. Gu, C.-G. Liu, S.-Y. Wang and S.-J. Ji, *J. Org. Chem.*, 2017, **82**, 2223–2230; (b) Z.-Y. Gu, Y. Liu, F. Wang, X. Bao, S.-Y. Wang and S.-J. Ji, *ACS Catal.*, 2017, **7**, 3893–3899; (c) P. Xu, T.-H. Zhu, T.-Q. Wei, S.-Y. Wang and S.-J. Ji, *RSC Adv.*, 2016, **6**, 32467–32470; (d) T.-H. Zhu, S.-Y. Wang, T.-Q. Wei and S.-J. Ji, *Adv. Synth. Catal.*, 2015, **357**, 823–828; (e) Q. Gao, P. Zhou, F. Liu, W.-J. Hao, C. Yao, B. Jiang and S.-J. Tu, *Chem. Commun.*, 2015, **51**, 9519–9522; (f) T.-H. Zhu, X.-P. Xu, G.-N. Wang, J.-J. Cao, T.-Q. Wei, S.-Y. Wang and S.-J. Ji, *Adv. Synth. Catal.*, 2014, **356**, 509–518; (g) T.-H. Zhu, S.-Y. Wang, Y.-Q. Tao, T.-Q. Wei and S.-J. Ji, *Org. Lett.*, 2014, **16**, 1260–1263.
- 7 (a) A. H. Shinde, S. Arepally, M. D. Baravkar and D. S. Sharada, *J. Org. Chem.*, 2017, **82**, 331–342; (b) G.-N. Wang, T.-H. Zhu, S.-Y. Wang, T.-Q. Wei and S.-J. Ji, *Tetrahedron*, 2014, **70**, 8079–8083.
- 8 S. Hayao, H. J. Haver, W. G. Strycker, R. A. Kulp and H. E. Hartzler, *J. Med. Chem.*, 1965, **8**, 807–815.
- 9 R. Villalobos-Molina, M. Ibarra and E. Hong, *Eur. J. Pharmacol.*, 1995, **277**, 181–185.
- 10 J. De Cree, J. Leempoels, H. Geukens, W. De Cock and H. Verhaegen, *Clin. Sci.*, 1981, **61**, 473S–476S.
- 11 T. F. Meert, C. J. E. Niemegeers, F. Awouters and P. A. Janssen, *Int. J. Drug Dev. Res.*, 1998, **13**, 327–332.
- 12 M. A. Geyer, N. R. Swerdlow, V. Lehmann-Masten, H.-J. Teschendorf, M. Traut and G. J. Gross, *J. Pharmacol. Exp. Ther.*, 1999, **290**, 716–724.
- 13 (a) M. E. Welsch, S. A. Snyder and B. R. Stockwell, *Curr. Opin. Chem. Biol.*, 2010, **14**, 347–361; (b) G. W. Rewcastle, In *Comprehensive Heterocyclic Chemistry III*, ed. A. R. Katritzky, C. A. Ramsden, E. F. V. Scriven and R. J. K. Taylor, Elsevier, Oxford, 2008.
- 14 (a) G. L. Beutner, Y. Hsiao, T. Razler, E. M. Simmons and W. Wertjes, *Org. Lett.*, 2017, **19**, 1052–1055; (b) E. Durham, D. Perkins, J. S. Scott, J. Wang and S. Watson, *Synlett*, 2016, 965–968.

- 15 NFPA 704 Health (H) rating: CO (H = 3), COCl₂ (H = 4), ClCO₂C₂H₅ (H = 4), Boc₂O (H = 3), isocyanates (e.g., *t*-BuNCO (H = 3)) and azides (H = 4) possess a high toxicity. Scale from 0 (low) to 4 (high).
- 16 (a) T. Zhang, Z. Wang, X. Hu, M. Yu, T. Deng, G. Li and H. Lu, *J. Org. Chem.*, 2016, **81**, 4898–4905; (b) B. Roberts, D. Liptrot, T. Luker, M. J. Stocks, C. Barber, N. Webb, R. Dods and B. Martin, *Tetrahedron Lett.*, 2011, **52**, 3793–3796; (c) N. Koay and L. C. Campeau, *J. Heterocycl. Chem.*, 2011, **48**, 473–478; (d) X. Q. Li, *Chin. Chem. Lett.*, 2009, **20**, 1201–1203; (e) M. C. Willis, R. H. Snell, A. J. Fletcher and R. L. Woodward, *Org. Lett.*, 2006, **8**, 5089–5091.
- 17 (a) W.-Z. Zhang, H. Li, Y. Zeng, X. Tao and X. Lua, *Chin. J. Chem.*, 2018, **36**, 112–118; (b) P. Mampuy, H. Neumann, S. Sergeyev, R. V. A. Orru, H. Jiao, A. Spannenberg, B. U. W. Maes and M. Beller, *ACS Catal.*, 2017, **7**, 5549–5556; (c) P. Xu, F. Wang, T.-Q. Wei, L. Yin, S.-Y. Wang and S.-J. Ji, *Org. Lett.*, 2017, **19**, 4484–4487.
- 18 (a) R. Paul, R. N. Gayen, S. Biswas, S. V. Bhat and R. Bhunia, *RSC Adv.*, 2016, **6**, 61661–61672; (b) R. Khatun, S. Biswas, M. S. Islam, I. H. Biswas, S. Riyajuddin, K. Ghosh and S. M. Islam, *ChemCatChem*, 2019, **11**, 1303–1312.
- 19 (a) C. C. Caliman, A. F. Mesquita, D. F. Cipriano, J. C. C. Freitas, A. A. C. Cotta, W. A. A. Macedo and A. O. Porto, *RSC Adv.*, 2018, **8**, 6136–6145; (b) A. Navaee and A. Salimi, *RSC Adv.*, 2015, **5**, 59874–59880; (c) D. C. Marcano, D. V. Kosynkin, J. M. Berlin, A. Sinitskii, Z. Sun, A. Slesarev, L. B. Alemany, W. Lu and J. M. Tour, *ACS Nano*, 2010, **4**, 4806–4814.
- 20 S. Wang, J. Wang, W. Zhang, J. Ji, Y. Li, G. Zhang, F. Zhang and X. Fan, *Ind. Eng. Chem. Res.*, 2014, **53**, 13205–13209.
- 21 (a) S. Rana and S. B. Jonnalagadda, *RSC Adv.*, 2017, **7**, 2869–2879; (b) Y. J. Li, W. Gao, L. J. Ci, C. M. Wang and P. M. Ajayan, *Carbon*, 2010, **48**, 1124–1130.
- 22 S. Rana, S. Maddila and S. B. Jonnalagadda, *Catal. Sci. Technol.*, 2015, **5**, 3235–3241.
- 23 (a) J.-B. Wu, M.-L. Lin, X. Cong, H.-N. Liu and P.-H. Tan, *Chem. Soc. Rev.*, 2018, **47**, 1822–1873; (b) J. L. E. Campos, H. Miranda, C. Rabelo, E. Sandoz-Rosado, S. Pandey, J. Riikonen, A. G. Cano-Marqueze and A. Jorio, *J. Raman Spectrosc.*, 2018, **49**, 54–65.
- 24 (a) S. Yang, W. Yue, J. Zhu, Y. Ren and X. Yang, *Adv. Funct. Mater.*, 2013, **23**, 3570–3576; (b) A. Kumar, L. Rout, R. S. Dhaka, S. L. Samala and P. Dash, *RSC Adv.*, 2015, **5**, 39193–39204; (c) L. Ma, X. Shen, J. Zhu, G. Zhu and Z. Ji, *J. Mater. Chem. A*, 2015, **3**, 11066–11073.
- 25 (a) S. Kumar, R. K. Yadav, K. Ram, A. Aguiar, J. Koh and A. J. F. N. Sobral, *J. CO₂ Util.*, 2018, **27**, 107–114; (b) Z. Li, S. Wu, D. Zheng, J. Liu, H. Liu, H. Lu, Q. Huo, J. Guan and Q. Kan, *Organomet. Chem.*, 2014, **28**, 317–323.
- 26 P. Hohenberg and W. Kohn, *Phys. Rev.*, 1964, **136**, B864–B871.
- 27 J. P. Perdew, *Unified Theory of Exchange and Correlation Beyond the Local Density Approximation, in Electronic Structure of Solids '91*, ed. P. Ziesche and H. Eschrig, Akademie Verlag, Berlin, 1991, pp. 11–20.
- 28 J. P. Perdew, *Phys. Rev. B: Condens. Matter Mater. Phys.*, 1992, **46**, 6671–6687.
- 29 (a) A. Bag and P. K. Ghorai, *RSC Adv.*, 2015, **5**, 31575–31583; (b) M. Sengupta, A. Bag, S. Ghosh, P. Mondal, A. Bordoloi and S. M. Islam, *J. CO₂ Util.*, 2019, **34**, 533–542.
- 30 B. Yu, J.-N. Xie, C.-L. Zhong, W. Li and L.-N. He, *ACS Catal.*, 2015, **5**, 3940–3944.